



B Flavor tagging with opposite-side soft electrons

The DØ Collaboration
URL: <http://www-d0.fnal.gov>

(Dated: July 17, 2005)

In this note, we present two analyses which study the use of soft electrons to tag the flavor of B hadrons. We first describe the feasibility of using opposite-side electrons for flavor tagging of B mesons, by utilizing a clean sample of fully reconstructed $B^\pm \rightarrow J/\psi K^\pm$ decays. From this study, we obtain a tag rate, $\epsilon = (2.0 \pm 0.2)\%$, tag purity, $\eta_s = (70.6 \pm 6.2)\%$ and dilution, $\mathcal{D} = 2\eta_s - 1 = (41 \pm 12)\%$. This translates to a tagging power, $\epsilon\mathcal{D}^2 = (0.34 \pm 0.19)\%$

We then apply this technique to a high statistics semileptonic B decay sample corresponding to approximately 417 pb^{-1} of integrated luminosity accumulated with the DØ Detector in Run II, and extract ϵ , \mathcal{D} and Δm_d . The flavor of the B_d^0 meson at decay was determined using the muon charge from the partially reconstructed decay $B_d^0 \rightarrow \mu^+ D^*(2010)^- X$, $D^*(2010)^- \rightarrow \bar{D}^0 \pi^-$, $\bar{D}^0 \rightarrow K^+ \pi^-$, whereas the initial state flavor was determined using opposite-side electrons. This yields tag rate, purity and dilution of,

$$\epsilon = (2.5 \pm 0.1)\%, \quad \eta_s = (66.9 \pm 1.5 \pm 0.5)\%, \quad \mathcal{D} = (34.0 \pm 3.0 \pm 0.9)\%$$

and tagging power, $\epsilon\mathcal{D}^2 = (0.29 \pm 0.05 \pm 0.03)\%$. The B_d^0 meson oscillation frequency was measured to be consistent with the world average and is an important first step to using the electron tag for a B_s oscillation measurement.

I. INTRODUCTION

The study of flavor oscillations in neutral B mesons is an important topic in heavy flavor physics. The measurement of the oscillation parameter Δm_d can be used to determine the product of the CKM matrix elements $|V_{tb}V_{td}^*|^2$, see [1] for a recent overview of the subject (a similar diagram holds for the B_s^0). Although, Δm_d has been measured very precisely by the B-factories at SLAC and KEK (world average [2] is $\Delta m_d = 0.502 \pm 0.007 \text{ ps}^{-1}$) theoretical uncertainties limit the precision on V_{td} to $\approx 15 - 17\%$. We can reduce the size of these uncertainties by combining Δm_d with a measurement of Δm_s . The observation of oscillations in the B_s system is a major goal of the Tevatron physics program.

A crucial ingredient in oscillations analyses is the knowledge of the flavor of the decaying meson at *production*. In this note, we present a flavor tagging algorithm using soft electrons. We first describe a feasibility study using fully reconstructed B^\pm events followed by an analysis which exploits a large semileptonic sample. Due to stricter selection criteria, the latter sample corresponds to approximately 417 pb^{-1} of integrated luminosity accumulated by DØ during the period from April 2002 to August 2004, whereas the feasibility study uses 460 pb^{-1} . B hadrons were selected using their semileptonic decays $B \rightarrow \mu^\pm D^{*-} X$ (charge conjugated states are always implied in this paper) with reconstructed $D^{*-} \rightarrow \bar{D}^0 \pi^-$ decays. Both simulation and available experimental results show that this sample is dominated by $B_d^0 \rightarrow \mu^+ \nu D^{*-} X$ decays and can therefore be used to study oscillations of neutral B mesons.

In Section II, we describe the DØ detector, in particular the sub-systems crucial for this analysis, and Section III explains how the data were collected. In Section IV, we briefly explain the soft electron tagging algorithm followed by a feasibility study performed using $B^\pm \rightarrow J/\psi K^\pm$ events. Section V has details on the reconstruction of the final state, both untagged and tagged samples. Sections VI and VII have details on the fitting procedure and extraction of Δm_d .

II. DETECTOR DESCRIPTION

The following main elements of the DØ detector are essential for this analysis:

- A magnetic central-tracking system, which consists of a silicon microstrip tracker (SMT) and a central fiber tracker (CFT), both located within a 2 T superconducting solenoidal magnet
- Calorimeter and a pre-shower subsystems for electron identification
- A muon system located beyond the calorimetry

The SMT has $\approx 800,000$ individual strips, with typical pitch of $50 - 80 \mu\text{m}$, and a design optimized for tracking and vertexing capability at $|\eta| < 3$. The system has a six-barrel longitudinal structure, each with a set of four layers arranged axially around the beam pipe, and 16 radial disks. The CFT has eight thin coaxial barrels, each supporting two doublets of overlapping scintillating fibers of 0.835 mm diameter, one doublet being parallel to the collision axis, and the other alternating by $\pm 3^\circ$ relative to the axis. Light signals are transferred via clear light fibers to solid-state photon counters (VLPC) that have $\approx 80\%$ quantum efficiency.

In between the solenoid magnet and calorimetry lies the preshower detector; the part which is in the central region ($|\eta| < 1.1$) is known as the CPS. Both central and forward preshower systems consist of several layers of extruded triangular shaped scintillators, which are read out by the same VLPC system as the CFT.

The liquid argon/uranium calorimeter consists of both electromagnetic (EM) and hadronic components [5], and extends out to $|\eta| \approx 4$ ($\eta = -\ln(\tan(\theta)/2)$, where θ is measured relative to the beam axis). In this analysis, we are primarily interested in the EM component, which form the first four layers (or “floors”) of the calorimeter.

The muon system consists of a layer of tracking detectors and scintillation trigger counters before 1.8 T toroids, followed by two additional layers after the toroids. Tracking at $|\eta| < 1$ relies on 10 cm wide drift tubes, while 1 cm mini-drift tubes are used at $1 < |\eta| < 2$.

III. DATA SAMPLE

This analysis uses a large sample of $B \rightarrow \mu^\pm D^{*(2010)\mp} X$ events selected from all data available up to August 2004 after removing a period of bad preshower reconstruction. This corresponds to $\sim 417 \text{ pb}^{-1}$ integrated luminosity. The events used in this analysis were primarily triggered by a suite of inclusive single muon triggers. However, once the event has been collected, an explicit trigger requirement is made in the offline analysis. The other B in the event are

also decay semileptonically producing another muon or an electron in the event. In this analysis, we focus on the case where the other B gives rise to an electron; this electron is then used for initial state flavor tagging.

A complementary analysis using $B \rightarrow \mu$ as the initial state tag was done previously [4]. In the current analysis, we use the same techniques and fitting algorithms to extract Δm_d . The reconstruction of the semi leptonic final state uses many of the selection criteria developed for the muon analysis.

IV. INITIAL STATE FLAVOR TAGGING WITH ELECTRONS

A. Soft electron selection

The track-based electron identification algorithm exploits the granularity of the calorimeter; details can be found in [7]. In short, a track (found in the central tracking system) is extrapolated into the calorimeter, and the transverse energy deposited in the cells in a narrow “road” centered on the track is summed. At the moment, we restrict ourselves to the central calorimeter, $|\eta| < 1.1$.

The two main discriminants in soft electron identification are E/p and fraction of the total energy in the EM calorimeter (EMF), and they are defined as,

$$EMF = \frac{\sum_{\text{floornumber } i=1,2,3} E_T(i)}{\sum_{\text{all floors}} E_T(i)} \quad (1)$$

$$E/P = \frac{\sum_{\text{floornumber } i=1,2,3} E_T(i)}{P_T(\text{track})} \quad (2)$$

where $E_T(i)$ is the transverse energy within the road in floor i .

We have studied these variables for reconstructed soft electrons (from B hadrons) in a MC sample, and representative plots are shown in Fig. 1.

We have also studied the soft electron variables using conversions ($\gamma \rightarrow e^+e^-$) and K_S^0 decays to $\pi^+\pi^-$ in data. The e - π separation can be seen in Fig. 2.

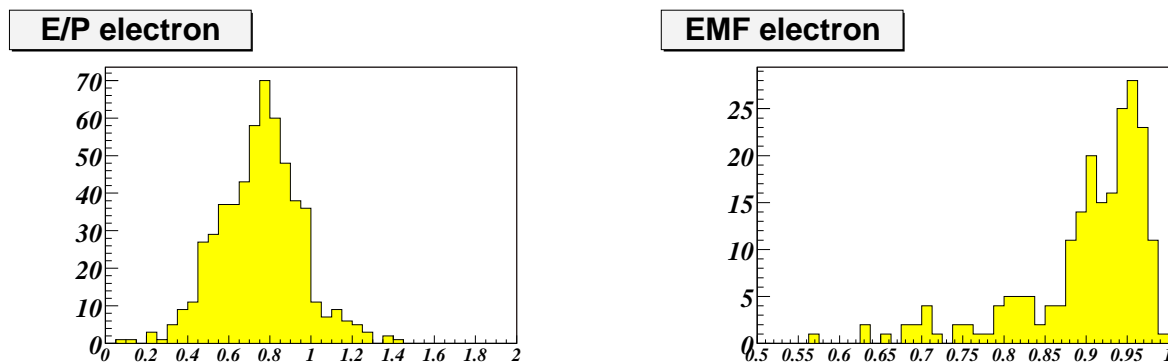


FIG. 1: $\frac{E}{P}$ and EMF of EM objects matched to generator level electrons ($|\eta| < 1.1$)

The ratio of energy contained in the “road” along the track to the total energy deposited in the first three floors of the calorimeter is 89% on the average. The energy deposited in the first three floors is 90% of the total energy deposited by the electron, so we expect $E/P \sim 80\%$ for road electrons, which agrees well with Fig. 1.

B. Benchmarking the electron tag algorithm

We first test the feasibility of using electrons as an initial state flavor tag by studying charged B mesons. Since B^\pm mesons do not mix, we use the electron charge to study the tag quality.

We reconstruct the decay $B^\pm \rightarrow J/\psi K^\pm$ using standard selection criteria [8]. In 460 pb^{-1} of integrated luminosity,

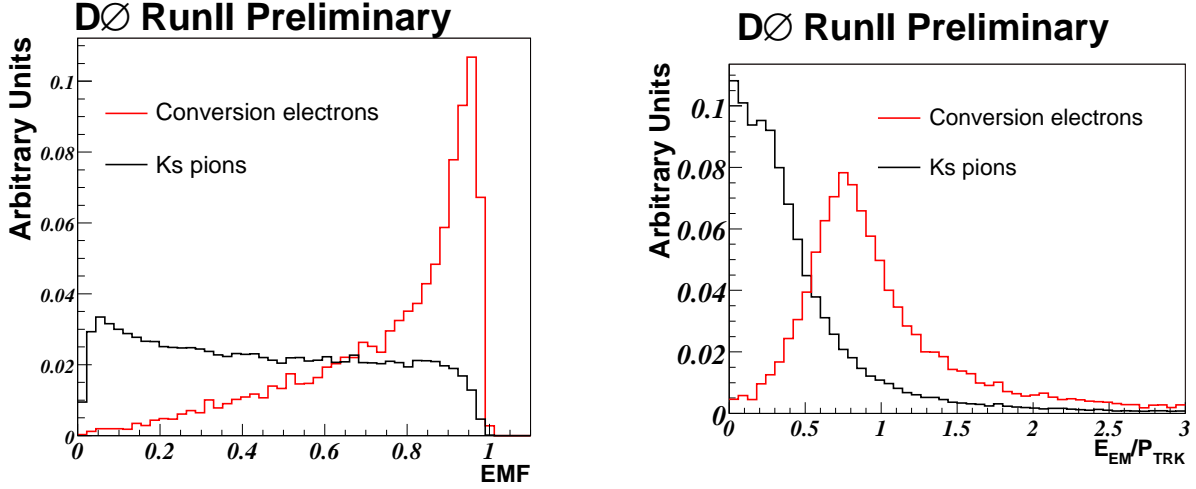


FIG. 2: $\frac{E}{P}$ and EMF of EM objects for pions from K_S decays and soft electrons ($2.0 < P_T < 20.0$ GeV/c) from photon conversion decays in the central region ($|\eta| < 1.1$).

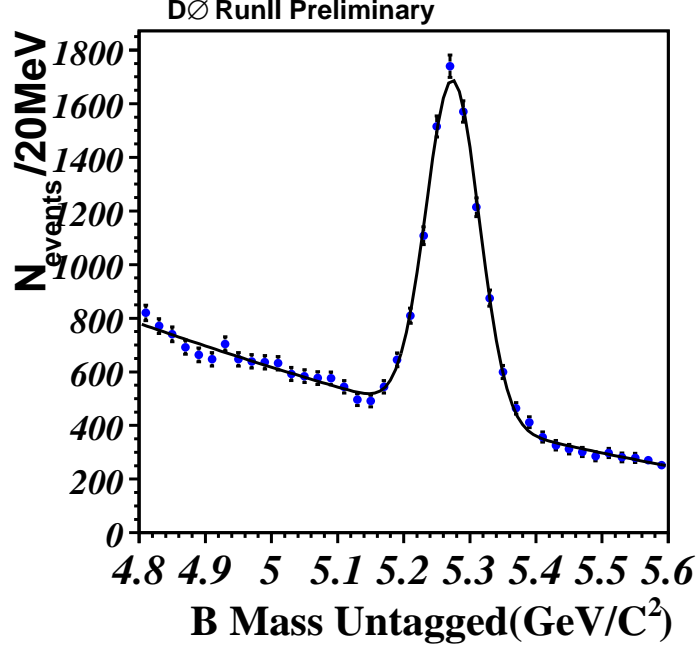


FIG. 3: Total number of flavor untagged B^\pm candidates

- Fiducial volume: Electron $|\eta| < 1.1$ and $P_T > 2.0$ GeV/c
- Select good electrons while discriminating against pions: $EMF > 0.7$ and $0.6 < E/P < 1.2$
- Angle between electron and the B candidate should be $|\phi| > 2.5$ rad(144°). This requirement forces the B hadrons to be well separated.

Currently, we restrict ourselves to the central region, since the background from photon conversions is quite large

Since the desired tag electron is produced in the semi-leptonic decay of a B hadron, it will tend to be associated with the jet created by the other daughters of the B hadron. The track jet is constructed only out of charged particles and uses the DURHAM clustering algorithm [6].

Thus, we look for non-isolated EM candidates; such EM candidates are within a cone of $\Delta R < 0.7$, where, $\Delta R = \sqrt{(\Delta\eta^2 + \Delta\phi^2)}$ where $\Delta\eta$ is the difference in η between electron and jet and $\Delta\phi$ is the difference in ϕ between electron and jet.

If we find more than one non-isolated EM candidate, we choose the electron with the maximum P_T^{rel} which is defined as the relative P_T of the electron with respect to the nearest jet (since a B hadron is heavier than other sources of soft electrons, on average, P_T^{rel} is larger). If no non-isolated electron is found, we take the electron with the maximum P_T . 5.7% of the tagged events containing a fully reconstructed B^\pm have more than 1 EM candidate.

Once we select an electron in an event containing $B^\pm \rightarrow J/\psi K^\pm$, we now have a tagged sample. The ratio of the number of events in the tagged sample to the total sample (N) is the tag rate (also referred to as the efficiency of the tag), ϵ . Since a charged B meson does not mix, the combination B^+e^- corresponds to a right sign tag (R), whereas B^+e^+ corresponds to a wrong sign tag (W). The variables, ϵ (tag rate), η_s (purity) and \mathcal{D} (dilution) defined below characterize the performance of the tagger; the figure of merit is $\epsilon\mathcal{D}^2$.

$$\epsilon = \frac{R+W}{N} \quad \eta_s = \frac{R}{R+W} \quad \mathcal{D} = \frac{R-W}{R+W} \quad (3)$$

In this analysis, we find 89 ± 12 and 37 ± 10 as the number of right-sign and wrong-sign tags, respectively. These yield $\epsilon = (2.0 \pm 0.2)\%$, $\mathcal{D} = (41.2 \pm 12.0)\%$, and $\epsilon\mathcal{D}^2 = (0.34 \pm 0.19)\%$, respectively. These numbers agree with a similar analysis done on MC events. The performance of the electron tagger, although not as good as the muon tagger (where $\epsilon\mathcal{D}^2 \sim 1\%$), is very encouraging, since it allows us to increase the statistics in our tagged sample by about 35% without any cost in trigger bandwidth or any other resources.

Now that we have demonstrated the feasibility of using an initial state electron tagger, we now turn to the measurement of Δm_d using $B_d^0 \rightarrow \mu^+ \nu D^{*-} X$ events.

V. FINAL STATE RECONSTRUCTION

A. Untagged sample

For this analysis, muons were required to have transverse momentum $P_T^\mu > 2$ GeV/c as measured in the central tracker, pseudo-rapidity $|\eta^\mu| < 2$ and total momentum $p^\mu > 3$ GeV/c.

All charged particles in a given event were clustered into jets using the DURHAM clustering algorithm [6]. Events with more than one identified muon in the same jet were rejected, as well as events with identified $J/\psi \rightarrow \mu^+ \mu^-$ decays.

The \bar{D}^0 candidate was constructed from two particles of the opposite charge belonging to the same jet as the reconstructed muon. Both particles are required to have transverse momentum $P_T > 0.7$ GeV/c, and pseudo-rapidity $|\eta| < 2$. They were required to form a common D -vertex with good fit χ^2 . For each particle, the axial (plane perpendicular to the beam direction) ϵ_T and stereo (plane parallel to the beam direction) ϵ_L projections of the track impact parameter with respect to the primary vertex together with the corresponding errors ($\sigma(\epsilon_T)$, $\sigma(\epsilon_L)$) were computed. The combined significance $\sqrt{(\epsilon_T/\sigma(\epsilon_T))^2 + (\epsilon_L/\sigma(\epsilon_L))^2}$ was required to be greater than 2. The distance d_T^D between the primary and D vertices in the axial plane was required to exceed 4 standard deviations: $d_T^D/\sigma(d_T^D) > 4$. The accuracy of the distance d_T^D determination was required to be better than 500 μm . The angle α_T^D between the \bar{D}^0 momentum and the direction from the primary to the \bar{D}^0 vertex in the axial plane was required to satisfy the condition: $\cos(\alpha_T^D) > 0.9$.

The tracks of muon and \bar{D}^0 candidate were required to form a common B -vertex with good fit χ^2 . The momentum of the B -candidate was computed as the sum of the momenta of the μ and \bar{D}^0 . The mass of the $(\mu^+ \bar{D}^0)$ system was required to fall within $2.3 < M(\mu^+ \bar{D}^0) < 5.2$ GeV/c². If the distance d_T^B between the primary and B vertices in the axial plane exceeded $4\sigma(d_T^B)$, the angle α_T^B between the B momentum and the direction from the primary to the B -vertex in the axial plane was demanded to satisfy the condition $\cos(\alpha_T^B) > 0.95$. The distance d_T^B was allowed to be greater than d_T^D , provided that the distance between the B and D vertices d_T^{BD} was less than $3\sigma(d_T^{BD})$. The error $\sigma(d_T^B)$ was required to be less than 500 μm .

The masses of kaon and pion were assigned to the particles according to the charge of the muon, requiring the

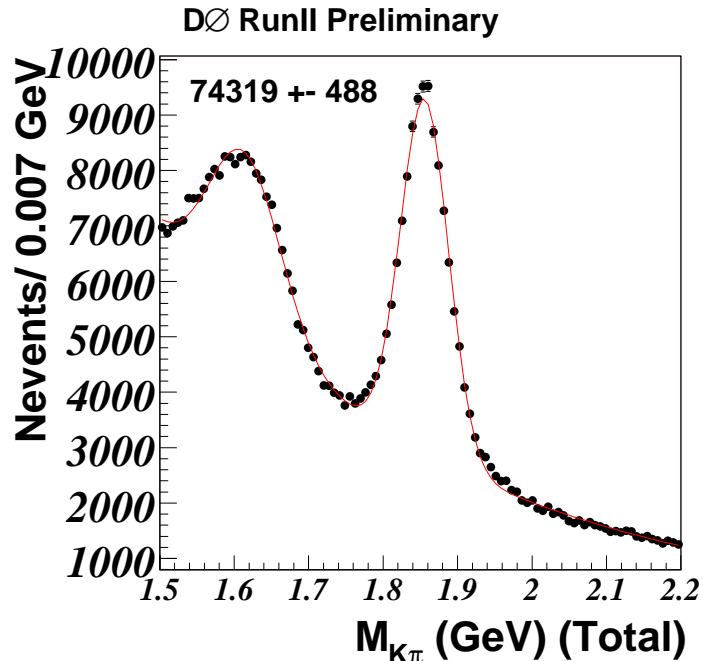


FIG. 4: The invariant mass of the $K\pi$ system for $\mu^+K^+\pi^-$ candidates before electron tagging. The curve shows the result of the fit of the $K^+\pi^-$ mass distribution with a Gaussian signal peak and polynomial background. The total number of D^0 candidates in the peak is 74319 ± 488 . The peak at lower masses corresponds to the partially reconstructed decay $\bar{D} \rightarrow K^+\pi^-X$ where typically a π^0 is not detected.

a $\mu^+K^+\pi^-$ final system. In the following the events falling into the $K\pi$ invariant mass window between 1.4 and 2.2 GeV/c^2 will be referred to as $\mu^+\bar{D}^0$ candidates.

The curve in Fig.4 shows the result of the fit of the $K^+\pi^-$ mass distribution with a Gaussian signal peak and polynomial background. The total number of D^0 candidates in the peak is 74319 ± 488 . The peak at lower masses corresponds to the partially reconstructed decay $\bar{D} \rightarrow K^+\pi^-X$ where typically a π^0 is not detected. With the tagging criteria described in the next section, the total number of electron tagged events is 1790 ± 96 which gives a tag rate of $(2.4 \pm 0.1\%)$.

For $\mu^+\bar{D}^0$ candidates, we search for an additional pion with charge opposite to the charge of muon and with $P_T > 0.18 \text{ GeV}/c$. The mass difference $\Delta M = M(\bar{D}^0\pi) - M(\bar{D}^0)$ for all such pions when $1.75 < M(\bar{D}^0) < 1.95 \text{ GeV}/c^2$ is shown in Fig.5. The peak, corresponding to the production of μ^+D^{*-} is clearly seen. The total number of D^* candidates in the peak is equal to 36086 ± 254 . The signal and the background have been modelled by a sum of two Gaussian functions and by the sum of exponential and first-order polynomial functions, respectively.

B. Tagged Sample

We now apply the electron tagging algorithm described in Section IV to the semi-leptonic final state. Since the semi-leptonic final state are primarily found in events collected with the inclusive single muon triggers, the event environment is likely to be different than in events with the J/ψ final state, which are collected with the dimuon trigger, we re-visit the electron selection criteria. The J/ψ events are less affected by noise, background *etc.* and tend to be “cleaner”.

The requirements for the electron tag are summarized below:

- Electron $|\eta| < 1.1$ and $P_T > 2.0 \text{ GeV}/c$
- The track associated with the electron has to have at least one hit in the Silicon detector
- To separate the tag electron from the decaying B candidate, we require (a) the electron is not from the same jet as the B candidate, and (b) $\cos(\theta)$ (angle between B and tag electron) < 0.5 .

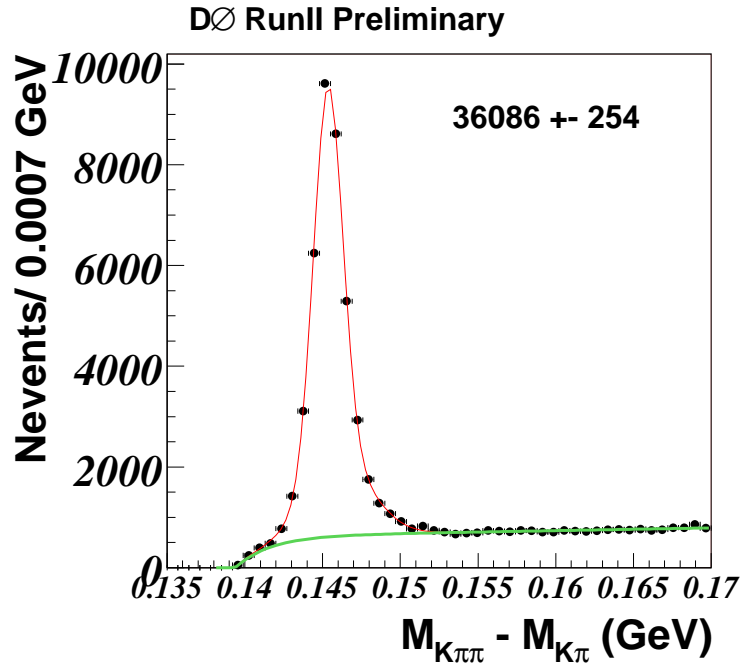


FIG. 5: The mass difference $M(D^0\pi) - M(D^0)$ for events with $1.75 < M(D^0) < 1.95$ GeV/ c^2 . Total number of D^* candidates is found to be 36086 ± 254 . In the fit function the signal and the background have been approximated respectively by sum of two Gaussian functions and by the sum of exponential and first order polynomial function, respectively.

- Electron does not come from a photon conversion or from a mis-identified pion (where the latter comes from K_S decay)
- The electron is well reconstructed in the preshower sub-detector. Reconstruction involves combining clusters in each of its three layers to form a 3D cluster. Fig. 6 shows the minimum single layer cluster (SLC) energy of a CPS cluster for electrons and pions. We have included a cut on this variable for tagging the semileptonic decays. A small part of the data had bad preshower reconstruction due to calibration problems, and has been removed.
- The electron satisfies criteria described in Table I. To improve electron identification, we have divided up the sample in 2 P_T bins and cuts are chosen to keep the pion rejection at the same level. This was studied using a sample of pions from K_S decays and conversions to e^+e^- .

Variable	$P_T^e < 3.5$ GeV/c	$P_T^e > 3.5$ GeV/c
E/P	> 0.55 & < 1.0	> 0.5 & < 1.1
EMF	> 0.8	> 0.7
Min CPS SLC_E (MeV)	> 4.0	> 2.0

TABLE I: Table summarizing the soft electron cuts.

As described in Section IV, if more than one non-isolated electron candidate per event is found the candidate with the maximum P_T^{rel} is selected. If no non-isolated electron is found, then the maximum P_T isolated electron is chosen.

Fig. 7 shows the mass difference $M(D^0\pi) - M(D^0)$ after tagging. It is found to be equal to 904 ± 36 and thus the tagging rate is determined to be $(2.5 \pm 0.1\%)$.

As will be described in Sec.VI the measurement of the B_d oscillations is performed using the ratio of D^* events with right and wrong tags. We also use the fits to the D^0 sample and do a simultaneous fit to obtain the mixing parameter. We use the same algorithm as the one used in the analysis with muons as the initial state flavor tag [4].

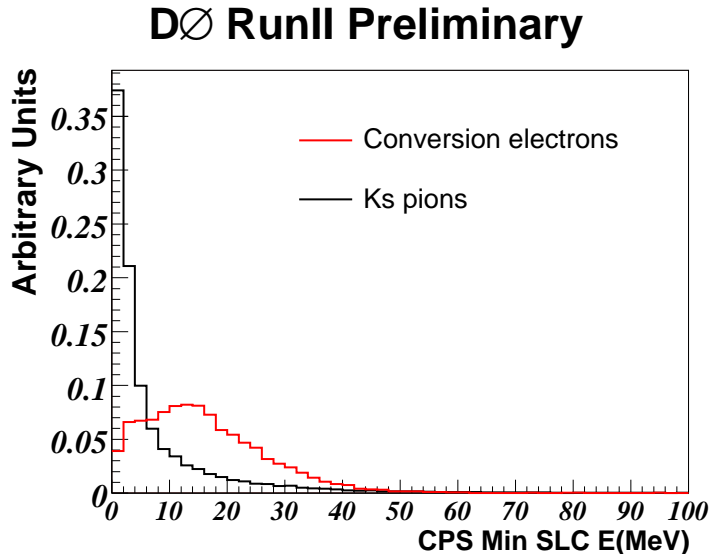


FIG. 6: Minimum CPS Single Layer Cluster energy of electrons (from photon conversions) and pions (from K_S^0 decays)

VI. EXPERIMENTAL OBSERVABLES

For a mixing analysis, we need to know the production and decay points of the B hadron, so that we can measure its decay length. The transverse decay length of a B -hadron L_{xy} was defined as the distance in the axial plane between the primary vertex and vertex produced by the muon and \bar{D}^0 . The vertexing algorithm is described in detail in [9].

The transverse momentum of a B -hadron $P_T^{\mu\bar{D}^0}$ was defined as the vector sum of transverse momenta of muon and \bar{D}^0 . The sign of the decay length was set positive, if the angle α_T^B was less than $\pi/2$, otherwise it was set negative. The measured *visible proper decay length* (VPDL) was defined as

$$x^M = L_{xy} \cdot M_B \cdot c / P_T^{\mu\bar{D}^0} \quad (4)$$

Events were divided into 7 bins according to the measured VPDL. The number of μ^+D^* events with same-sign (“oscillated”) and opposite-sign (“non-oscillated”) tags, N_i^{osc} and $N_i^{non-osc}$, in each bin i of VPDL were determined from a fit of the D^* peak in the mass difference $M(D^0\pi) - M(D^0)$ distribution.

Bin	VPDL range, cm	N_{tot}	$N_i^{non-osc}$	N_i^{osc}	ϵ_i	A_i	A_i^e
1	-0.025-0.000	2154 ± 61	29 ± 6	14 ± 5	2.00 ± 0.30	0.359 ± 0.170	0.340
2	0.000-0.025	9974 ± 212	159 ± 14	88 ± 10	2.48 ± 0.16	0.286 ± 0.067	0.331
3	0.025-0.050	8832 ± 137	125 ± 12	59 ± 9	2.09 ± 0.15	0.355 ± 0.078	0.287
4	0.050-0.075	6156 ± 121	76 ± 9	46 ± 8	1.98 ± 0.18	0.245 ± 0.096	0.207
5	0.075-0.100	4163 ± 88	51 ± 8	49 ± 7	2.39 ± 0.24	0.025 ± 0.109	0.104
6	0.100-0.125	2930 ± 140	27 ± 6	25 ± 6	1.77 ± 0.24	0.034 ± 0.157	-0.003
7	0.125-0.250	4735 ± 111	49 ± 8	67 ± 9	2.45 ± 0.23	-0.163 ± 0.104	-0.151

TABLE II: Definition of the seven bins in VPDL. For each bin the measured number of D^* for the opposite sign and same sign of muon tag $N_i^{non-osc}$, N_i^{osc} , its statistical error $\sigma(N_i^{non-osc})$; $\sigma(N_i^{osc})$, all determined from the fits of corresponding mass difference $M(D^0\pi) - M(D^0)$ distributions, measured asymmetry A_i , its error $\sigma(A_i)$ and expected asymmetry A_i^e corresponding to $\Delta m_d = 0.545 \text{ ps}^{-1}$ (the fit result) are given.

The experimental observables, asymmetry A_i in each VPDL bin, for this measurement were defined as:

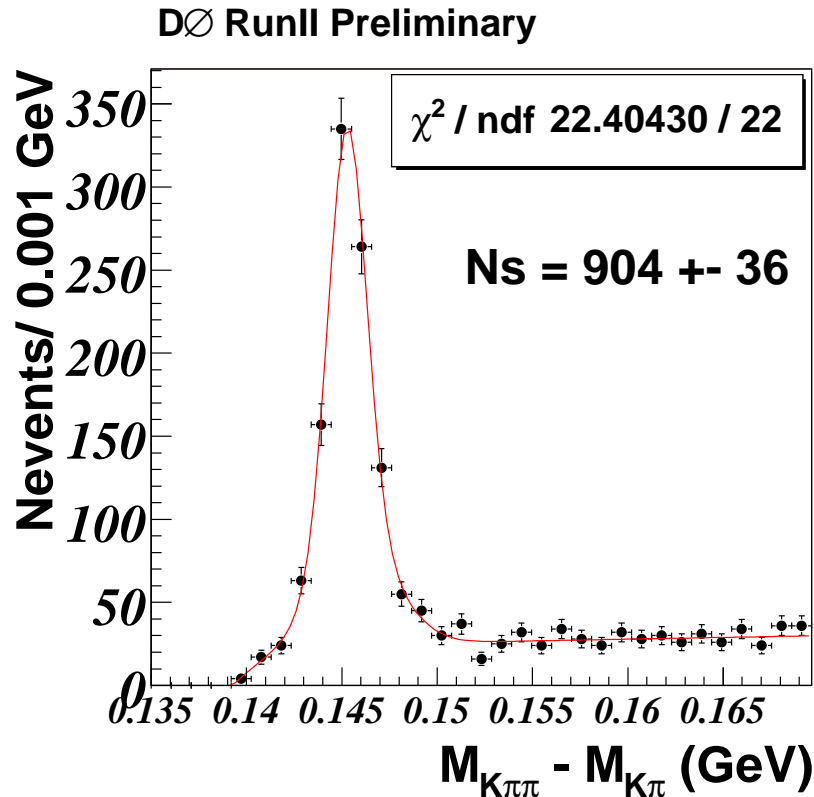


FIG. 7: The mass difference $M(D^0\pi) - M(D^0)$ for tagged events with $1.75 < M(D^0) < 1.95 \text{ GeV}/c^2$. The tag rate is found to be $(2.50 \pm 0.1)\%$

The number of “non-oscillated” and “oscillated” events, the asymmetries and the corresponding errors derived from the fit in each VPDL bin are given in Table II. For comparison, we show the expected asymmetry obtained from the best fit to the data (described in Section VII). Fig. 8 shows the asymmetry as a function of the visible proper decay length.

VII. FITTING PROCEDURE AND RESULTS

The D^* sample is composed mostly of B_d^0 mesons with some contributions from B_u and B_s mesons. Different species of B mesons behave differently with respect to oscillations. Neutral B_d^0 and B_s mesons do oscillate while charged B_u mesons do not oscillate. In the following it was assumed that the oscillations of B_s mesons have infinite frequency. Possible contributions from b-baryons to the sample were also neglected.

The purity of the tagging method was defined as $\eta_s = N_{\text{correctly tagged events}}/N_{\text{total tagged events}}$. It was assumed that the tagging purity is the same for all reconstructed B mesons because the opposite-side tagging information has little correlation with the reconstructed B meson candidate.

For a given type of reconstructed B-hadron (i.e. d , u , s), the distribution of the visible proper decay length x is given by:

$$n_d^{non-osc}(x, K) = \frac{K}{c\tau_{B_d}} \exp\left(-\frac{Kx}{c\tau_{B_d}}\right) \cdot 0.5 \cdot (1 + (2\eta_s - 1) \cos(\Delta m \cdot Kx/c));$$

$$n_d^{osc}(x, K) = \frac{K}{c\tau_{B_d}} \exp\left(-\frac{Kx}{c\tau_{B_d}}\right) \cdot 0.5 \cdot (1 - (2\eta_s - 1) \cos(\Delta m \cdot Kx/c)); \quad (6)$$

$$n_u^{non-osc}(x, K) = \frac{K}{c\tau_{B_u}} \exp\left(-\frac{Kx}{c\tau_{B_u}}\right) \cdot \eta_s; \quad n_u^{osc}(x, K) = \frac{K}{c\tau_{B_u}} \exp\left(-\frac{Kx}{c\tau_{B_u}}\right) \cdot (1 - \eta_s); \quad (7)$$

$$n_s^{non-osc}(x, K) = n_s^{osc}(x, K) = \frac{K}{c\tau_{B_s}} \exp\left(-\frac{Kx}{c\tau_{B_s}}\right) \cdot 0.5, \quad (8)$$

where $K = P_T^{\mu D^0}/P_T^B$ is a K -factor reflecting the difference between the observable and true momentum of the B -hadron and τ is the lifetime of B -hadrons taken from [2]. The K -factors were determined from the simulation using generator-level information for the computation of p_T^B and $P_T^{\mu D^0}$. The following decay channels of B mesons were considered: $B_d^0 \rightarrow \mu^+ \nu D^{*-}$, $B_d^0 \rightarrow \mu^+ \nu D^{**} \rightarrow \mu^+ \nu D^{*-} X$, $B^+ \rightarrow \mu^+ \nu \bar{D}^{*0} \rightarrow \mu^+ \nu D^{*-} X$ and $B_s^0 \rightarrow \mu^+ \nu D^{*-} X$. Here and in the following the symbol “ D^{**} ” denotes both narrow and wide D^{**} resonances, together with non-resonant $D\pi$ and $D^* \pi$ production. The slow pion from D^{*-} -decay was not included in the $P_T(\mu D^0)$ computation for the K -factors. The K -factors for all considered decays were combined into 3 groups: $B \rightarrow \mu^+ \nu \bar{D}^* X$, $B \rightarrow \mu^+ \nu \bar{D}^{**} X \rightarrow \mu^+ \nu \bar{D}^* X$ and $B_s \rightarrow \mu^+ \nu \bar{D}^* X$.

Translation to the measured VPDL, x^M is achieved by integration over K -factors and resolution functions:

$$N_{(d,u,s),j}^{osc, non-osc}(x^M) = \int dx Res_j(x - x^M) \cdot Eff_j(x) \int dK D_j(K) \cdot \theta(x) \cdot n_{(d,u,s),j}^{osc, non-osc}(x, K). \quad (9)$$

Here $Res_j(x - x^M)$ is the detector resolution of the VPDL and $Eff_j(x)$ is the reconstruction efficiency for a given decay channel j of this type of B meson. Both are determined from the simulation. The decay length resolution was parameterised by the sum of 3 Gaussians with the following parameters: widths 26, 56 and 141 microns; relative normalizations 0.423, 0.505 and 0.072 respectively. The step function $\theta(x)$ takes into account that only positive values of x are possible (x^M can have negative values due to resolution effects). The function $D_j(K)$ gives the normalized distribution of the K -factor in a given channel j .

The expected number of oscillated/non-oscillated events in the i -th bin of VPDL is equal to

$$N_i^{e,osc/non-osc} = \int_i dx^M \left(\sum_{f=u,d,s} \sum_j (Br_j \cdot N_{f,j}^{osc/non-osc}(x^M)) \right) \quad (10)$$

Here the integration $\int_i dx^M$ is taken over a given interval i , the sum \sum_j is taken over all decay channels $B \rightarrow \mu^+ \nu D^{*-} X$ and Br_j is the branching ratio of a given channel j .

The latest PDG values [2] were used for the B decay branching fractions. Exploiting the fact that semileptonic B decays are saturated by decays to D , D^* and D^{**} , and isotopical invariance it was determined that the B_d^0 (85%) and B^+ (15%) decays give the main contributions to the sample. The B_s contribution is small but it was taken into account.

Finally, the expected value A_i^e for interval i of the measured VPDL is given by Equation (5), and substituting $N_i^{non-osc}$ and N_i^{osc} by $N_i^{e,non-osc}$ and $N_i^{e,osc}$.

The fit values of Δm and η_s were determined from the minimization of a $\chi^2(\Delta m, \eta_s)$ defined as:

$$\chi^2(\Delta m, \eta_s) = \sum_i \frac{(A_i - A_i^e(\Delta m, \eta_s))^2}{\sigma^2(A_i)}. \quad (11)$$

We perform a simultaneous fit to the B^0 and B^+ samples. The result of the minimization is:

$$\Delta m_d = 0.545 \pm 0.085 \text{ (stat) ps}^{-1} \quad \eta_s = (66.9 \pm 1.5)\% \quad (12)$$

The values of A_i^e obtained in each bin are given in Table II. Fig. 8 shows the asymmetry as function of VPDL together with the result of the fit [10].

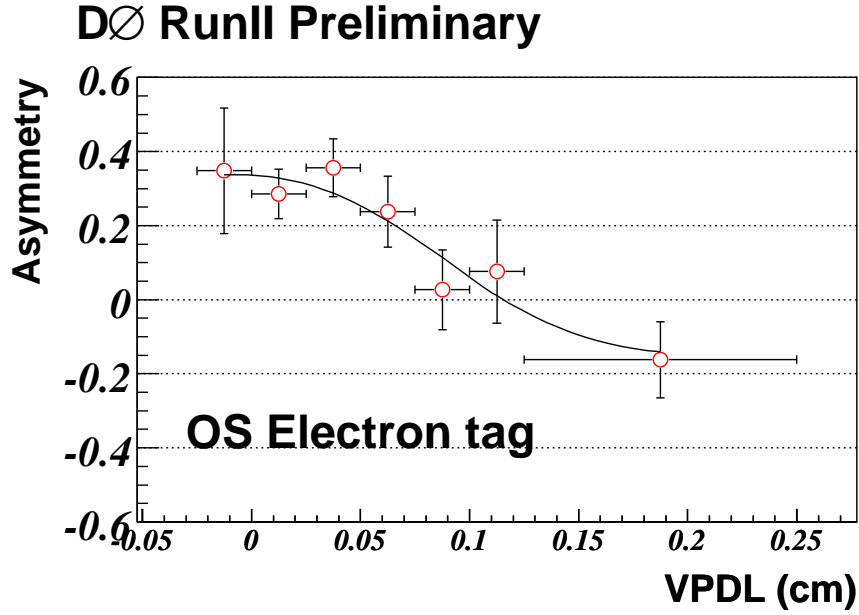


FIG. 8: The asymmetry in D^* sample (dominated by B^0) as a function of the visible proper decay length in cm. The result of the minimization of (11) with $\Delta m_d = 0.545 \text{ ps}^{-1}$ is shown as a curve.

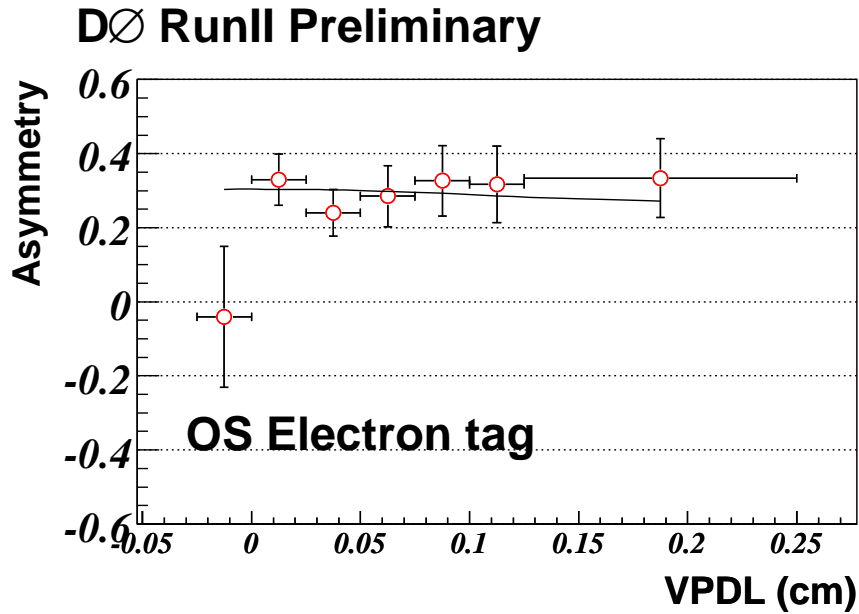


FIG. 9: The asymmetry in D^0 sample (dominated by B^+) as a function of the visible proper decay length in cm. The result of the minimization of (11) with $\Delta m_d = 0.545 \text{ ps}^{-1}$ is shown as a curve.

VIII. A STUDY OF SYSTEMATIC UNCERTAINTIES

We studied various sources of systematic uncertainties and the more important ones are described in this section, and results summarized in Table III.

The B meson branching rates and lifetimes used in the fit of the asymmetry were taken from [2] and were varied by 1σ . The VPD resolution, obtained in simulation, was multiplied by a large factor, from 0.2 to 2, which significantly exceeds the estimated difference in the resolution between data and simulation.

The variation of K -factors with the change of B momentum was neglected in this analysis. To check the impact of this assumption on the final result, their computation was repeated without the cut on $P_T(D^0)$ or by applying an additional cut on P_T of muon, $P_T > 4 \text{ GeV}/c$. The change of average value of K -factors did not exceed 2%, which was used as the estimate of the systematic uncertainty in their values. This was propagated into the variation of Δm_d and tagging purity by repeating the fit with the K -factor distributions shifted by 2%.

The reconstruction efficiency in different B -meson decay channels depends only on the kinematic properties of corresponding decays and can therefore be reliably estimated in the simulation. The ISGW2 model [11] was used to describe semileptonic B decays. The uncertainty of the reconstruction efficiency, set at 12%, was estimated by varying kinematic cuts on P_T of the muon and D^0 in a wide range. Changing the model describing semileptonic B decay from ISGW2 to HQET [12] produces a smaller variation. The fit to extract Δm_d was repeated with the efficiencies to reconstruct $B \rightarrow \mu^+ \nu D^{*-}$ and $B \rightarrow \mu^+ \nu \bar{D}^{*0}$ channels modified by 12%, and the difference was taken as the systematic uncertainty from this source.

Possible background contribution into events with small lifetime, e.g. the $c\bar{c}$ contamination of the sample or the misidentification of the muon, can bias the oscillation wave at small values of VPD. The contribution of this background was varied from 3.5% to 10% and the difference in the result was taken as the systematic uncertainty from this source.

We also investigated the systematic uncertainty of measuring the number of D^* and D^0 candidates in each VPD bin. This we call systematics due to fit procedure. We changed the background parametrization for the D^0 mass fit from the exponent to a second degree polynomial and varied the background shape by $\pm 1\sigma$.

For the D^* candidates, we performed cross-checks using other functions, but the chosen background parametrization gives the best description. Since we fix the background shape, we varied the background shape by $\pm 1\sigma$. Also, the default bin width for the fits in the fits in individual VPD bins is 1.40 MeV. We lowered the binwidth to 1.05 MeV, and increased the binwidth 1.75 MeV, and include it in our systematics.

	variation	$\delta(\Delta m_d)$	$\delta(\mathcal{D}(B^0))$	$\delta(\mathcal{D}(B^+))$	$\delta(\mathcal{D})$
$Br(B^0 \rightarrow D^{*-} \mu^+ \nu)$	$5.53 \pm 0.023\%$	0.002 ps^{-1}	0.001	0.001	0.001
$Br(B \rightarrow D^* \pi \mu \nu X)$	$1.07 \pm 0.17\%$	0.008 ps^{-1}	0.002	0.001	0.001
B lifetime	$\pm 1\sigma$	0.001 ps^{-1}	0.000	0.000	0.000
Resolution function	$\times [0.2 \div 2]$	0.006 ps^{-1}	0.002	0.000	0.000
Alignment	$\pm 10 \mu\text{m}$	0.007 ps^{-1}	0.004	0.000	0.004
K -factor	$\pm 2\%$	0.009 ps^{-1}	0.000	0.000	0.000
$c\bar{c}$ Background	$[0.035 \div 0.1]$	0.002 ps^{-1}	0.002	0.000	0.002
Efficiency	$\pm 12\%$	0.006 ps^{-1}	0.001	0.001	0.001
Fit procedure	Overall	0.010 ps^{-1}	0.006	0.006	0.008
Total		0.019 ps^{-1}	0.008	0.006	0.009

TABLE III: Systematic uncertainties.

IX. CONCLUSIONS

We report results for a new algorithm, which uses soft electrons, to tag the flavor of a B hadron at production. We use both fully reconstructed B^\pm events as well as a large semileptonic sample corresponding to about 36086 ($\mu^+ D^* X$) candidate events.

Using the latter sample, the B^0 meson oscillation frequency was measured to be consistent with the world average. We also obtained a tag rate, purity and dilution of,

$$\epsilon = (2.5 \pm 0.1)\% \quad n = (66.9 \pm 1.5 \pm 0.5)\% \quad \mathcal{D} = (34.0 \pm 3.0 \pm 0.9)\%$$

Acknowledgments

We thank the staffs at Fermilab and collaborating institutions, and acknowledge support from the Department of Energy and National Science Foundation (USA), Commissariat à L'Energie Atomique and CNRS/Institut National de Physique Nucléaire et de Physique des Particules (France), Ministry for Science and Technology and Ministry for Atomic Energy (Russia), CAPES, CNPq and FAPERJ (Brazil), Departments of Atomic Energy and Science and Education (India), Colciencias (Colombia), CONACyT (Mexico), Ministry of Education and KOSEF (Korea), CONICET and UBACyT (Argentina), The Foundation for Fundamental Research on Matter (The Netherlands), PPARC (United Kingdom), Ministry of Education (Czech Republic), Natural Sciences and Engineering Research Council and West-Grid Project (Canada), BMBF (Germany), A.P. Sloan Foundation, Civilian Research and Development Foundation, Research Corporation, Texas Advanced Research Program, and the Alexander von Humboldt Foundation.

-
- [1] Z.Ligetti “Introduction to heavy meson decays and CP asymmetries”, hep-ph/0302031.
 - [2] K. Hagiwara *et al.*, Phys. Rev. **D66**, 010001 (2002) and 2003 off-year partial update for the 2004 edition available on the PDG WWW pages (URL: <http://pdg.lbl.gov/>).
 - [3] E.Berger *et al.*, Phys. Rev. Lett. **86**, 4231 (2001).
 - [4] DØ Collaboration, “Flavor oscillations in B_d^0 mesons with opposite-side muon tags”. DØ Note 4370, Mar, 2004.
 - [5] S. Abachi *et al.*, Nucl. Instrum. Methods Res. **A 338** (185), 1994.
 - [6] S.Catani *et al.*, Phys. Lett. **B269** (1991) 432.
 - [7] F. Beaudette and J.-F. Grivaz, “The Road Method (an algorithm for the identification of electrons in jets)”, DØ Note 3976, Nov 4 2002.
 - [8] Reconstruction of B hadron signals at D0: <http://www-d0.fnal.gov/Run2Physics/WWW/results/prelim/B/B00/B00.pdf>.
 - [9] DELPHI Collab., *b-tagging in DELPHI at LEP*, Eur. Phys. J. **C32** (2004), 185-208.
 - [10] As a check the fit was performed by allowing different values of purity for the B^0 and B^+ dominated samples. In this case, we obtain η_s^0 and η_s^+ to be $(67.4 \pm 2.8)\%$ and $(66.8 \pm 2.0)\%$, respectively, which is consistent with the main result in the text.
 - [11] D. Scora and N. Isgur, Phys. Rev. D **52**, 2783 (1995).
 - [12] M. Neubert, Phys. Rep. **245**, 259 (1994).